



Analysis of naphthalene adsorption from wastewater using activated and non-activated biochar produced from bagasse

Shivangi Pathak¹ · K. K. Pant² · Priyanka Kaushal¹

Received: 5 January 2023 / Revised: 6 March 2023 / Accepted: 12 March 2023 / Published online: 27 May 2023
© The Author(s), under exclusive licence to Springer-Verlag GmbH Germany, part of Springer Nature 2023

Abstract

Wastewater containing polycyclic aromatic hydrocarbons (PAHs), when improperly managed or released into the environment, can disrupt the ecosystem and degrade the quality of water bodies. Wastewater that contains PAHs needs to be treated immediately. Bagasse was pyrolyzed in this work to produce alternate biochar, which was subsequently CO₂-activated. CO₂-activated and non-activated biochar were characterized and evaluated for adsorption of naphthalene from an aqueous solution. Thermodynamics, equilibrium, and adsorption kinetics studies were conducted. Contrary to non-activated biochar, which had a surface area of less than 71 m²/g, CO₂-activated biochar was a typical mesoporous material with a surface area of roughly 263 m²/g. Therefore, compared to non-activated biochar, CO₂-activated biochar has a more significant potential for naphthalene adsorption. CO₂-activated and non-activated biochar had maximal naphthalene adsorption capacities of 290.43 and 38.15 mg/g, respectively. According to the findings, both feedstocks achieved the optimal adsorption capacity at pH 7, and 0.2 g of adsorbent at 120 and 180 min for activated and non-activated biochar, respectively. Naphthalene adsorption on CO₂-activated biochar proceeded according to the pseudo-second-order model's kinetics. For CO₂-activated biochar, with consideration to the equilibrium adsorption isotherms, Langmuir offered the best match. Physical modification considerably enhanced the adsorption of naphthalene onto CO₂-activated biochar. Naphthalene and biochar were able to bind to one another by physical interaction, electrostatic attraction, hydrogen bonds, and π - π interaction. Naphthalene adsorption on CO₂-activated biochar was spontaneous, exothermic, and favorable. Hence, modified biochar (CO₂-activated) has the potential to produce a substitute mesoporous adsorbent from bagasse to remediate naphthalene from wastewater.

Keywords Pyrolysis · Biochar · CO₂ activation · Bagasse · Adsorption · Naphthalene

Abbreviations

ASB600 Activated biochar
BET Brunauer–Emmett–Teller

EPA Environmental Protection Agency
FTIR Fourier transform infrared
G° Gibbs free energy
H° Enthalpy
IS Indian Standard
NAP Naphthalene
PAH Polycyclic aromatic hydrocarbon
PZC Point of zero charge
SB600 Non-activated biochar
SEM Scanning electron microscope
S° Entropy
SB Sugarcane bagasse

Highlights

- Single step CO₂ activation of bagasse was studied.
- Surface areas of activated and non-activated biochar were 263.05 and 70.07 m²/g, respectively.
- More aromatic functional groups form with the increase in pyrolysis temperature.
- Adsorbent dose, pH, PAHs concentration, and contact time affect adsorption process.
- Langmuir model demonstrated good agreement with the adsorption isotherm for activated biochar.

✉ Priyanka Kaushal
priyankak@iitd.ac.in

¹ Centre for Rural Development and Technology, Indian Institute of Technology, Delhi, New Delhi 110116, India

² Department of Chemical Engineering, Indian Institute of Technology Roorkee, New Delhi 110016, India

1 Introduction

Increasing concerns about anthropogenic sources of water course contamination propel activated carbon. Various organic and inorganic contaminants dissolved in aqueous

or gaseous environments have been successfully removed using activated carbon [1]. However, the high price of activated carbon hinders its widespread application [2]. India has a large volume of agricultural waste, which offers distinct advantages as a source of raw materials and is gaining increasing research interest [3, 4]. Their great capabilities are directly related to the activated biochar surface's well-developed porous structures, substantial surface area, and a vast variety of functional groups. It is generally known that the surface functional groups of activated biochar can cause the surface to exhibit acidic, basic, or neutral properties [5]. To improve or increase the affinities of carbon materials for certain pollutants, attention has lately been focused on describing and changing their surface functional groups [2, 6, 7].

Bagasse, a typical biomass waste from the sugar industry, is still very difficult to dispose of. Reports claim that biomass waste can clean wastewater and improve soil [8–10]. Sugarcane bagasse can be immediately pyrolyzed to produce biochar, which has a 1.67 mmol/g CO₂ absorption capacity at 25 °C, according to research by Creamer et al. [11]. Most past studies have concentrated on employing different activating agents to create porous carbons with desirable physicochemical properties [12–14]. The activating agent would undoubtedly influence the effectiveness of PAHs adsorption and the textural characteristics of carbon adsorbents generated from sugarcane bagasse.

Organic pollutants with two or more fused aromatic rings of carbon and hydrogen are called polycyclic aromatic hydrocarbons (PAHs). Incomplete raw material burning in the coal and petrochemical industries, automobile exhaust emissions, and oil product leaks are common causes of their production. Because of their high toxicity, carcinogenicity, and stability, PAHs were identified by the US Environmental Protection Agency (EPA) as the primary contaminants [15, 16]. Due to their limited biodegradability, poor ionization ability, low water solubility, and high resistance to natural degradation processes, PAHs can travel long distances in the

air and water [17]. PAHs penetrate the human body and are easily absorbed by cells because of their high carbon content and hydrophobicity. Certain PAHs can interact with DNA, resulting in mutagenic and carcinogenic effects [75]. The coking of coal tar and the distillation of petroleum produce large amounts of naphthalene (NAP), the industry's most prominent fused aromatic hydrocarbon [18]. After NAP is released into a surface water body, a secondary pollutant is produced by diverse interactions in environmental species [19], endangering human health and the ecosystem [20]. As a result, it is critical to adopt cost-effective and efficient methods to reduce NAP contamination.

Numerous methods have been used in recent years to remove PAHs from wastewater [21–23], but adsorption is an adaptable, low-cost method that could raise water quality without introducing more contaminants, and the adsorbent can be reused [24]. Table 1 lists the drawbacks of each conventional method.

Biochar is a “carbon-rich solid substance” made by pyrolyzing biomass in an inert environment at high temperatures (300–600 °C) [11]. Compared to biomass, biochar is rich in carbon content, microporosity, and more surface functional groups [37]. The significant surface area, porous structure, and surface functional groups like carboxyl, hydroxyl, and phenolic in biochar give it an excellent adsorption capacity to remove contaminants [38]. Due to its versatility, affordability, low energy requirement, and environmental sustainability, adsorption utilizing biochar made from various agricultural leftovers has been identified as a viable green technology [39, 40]. Biomass resources (including agricultural waste, municipal solid waste, and animal and food waste [41]) have recently been employed as precursors to produce specific biochar materials due to their low cost and widespread availability. Using low-cost agricultural solid wastes opens up new opportunities to eliminate wastewater's organic pollutants [16, 42]. However, biochar has several restrictions when utilized as an adsorbent or in other environmental applications because of its limited surface area, low porosity, and confined surface functional

Table 1 Demerits of different methods used for PAHs removal

Techniques	Demerits	Reference
Coagulation	<ul style="list-style-type: none"> • Inefficient for removing organic contaminants • Sludge formation 	[25, 26]
Flocculation	<ul style="list-style-type: none"> • Production of secondary pollution • Requirement of nutrient for microbial development 	[26, 27]
Bioremediation	<ul style="list-style-type: none"> • Challenge of optimizing time is significant 	[28, 29]
Solid-phase extraction	<ul style="list-style-type: none"> • Expensive solvents • Harmful impact on environment 	[30, 31]
Solvent extraction	<ul style="list-style-type: none"> • Process is labor- and time-intensive • Less effective with low concentrations of contaminants 	[32, 33]
Chemical oxidations	<ul style="list-style-type: none"> • Maintenance and operational cost high 	[21, 31, 34–36]
Photocatalytic degradation	<ul style="list-style-type: none"> • Photocatalytic reactor maintenance cost high 	[8, 9]
Reverse osmosis	<ul style="list-style-type: none"> • Unprofitable for small- and medium-sized enterprises 	[10, 31]

groups. By using various activators and heating the biochar between 500 and 900 °C, the activation procedure enhances the physicochemical characteristics of the material. The type of adsorbent used determines how well particular pollutants are absorbed after being adsorbed [43]. According to the study “Global Activated Carbon Market Forecast & Opportunities 2017,” the growth rate of demand for activated carbon is predicted to be more than 10% per year over the ensuing 5 years, reaching a market value of \$3 billion by 2025 [44]. Activated biochar has been utilized extensively in adsorption techniques, which have the potential to be successful in the elimination of persistent organic pollutants [22, 24, 25, 75].

This study aims to develop CO₂-activated biochar, an intriguing material made from sugarcane residues like bagasse. We investigated the use of CO₂-activated biochar in place of adsorbents to remove NAP from aqueous media. Based on this idea, it is conceivable to create a synergistic effect in the field of waste management, i.e., the creation of substitute material from solid wastes like bagasse that may be used to treat aromatic hydrocarbon effluents. Bagasse was pyrolyzed with N₂ to create biochar, and further biochar was activated with CO₂. All three, the precursor, biochar, and activated biochar, were characterized. A batch system’s ability to adsorb naphthalene was evaluated using kinetic, equilibrium, and thermodynamic analyses of activated biochar produced from bagasse.

2 Materials and methodology

The raw material (bagasse) for the current study was purchased from a local Delhi, India, sugarcane juice shop. Before being dried for 3 days in the sun, the obtained material was cleansed with distilled water to remove any remaining dust. The feedstock was pre-dried before analysis to make it suitable for pyrolysis operations. This was done because pyrolysis is more energy-intensive when there is a high moisture content. It also lowers the pyrolyzer’s internal temperature and the output gas’s heating value. One to two kilograms of biomass were dried at 105 °C for 2 h in a hot air oven. To achieve a particle size of between 250 and 500 μm, the biomass was dried, crushed, and sieved using Indian Standard (IS) sieves. For intensive analysis, the biomass was then stored in a lab-controlled atmosphere.

Table 2 displays the physical characteristics analysis of bagasse. The ASTM E1755 and ASTM D3175 techniques were used to ascertain how much ash and volatile matter were present in the raw material. The mass difference method was

next applied to determine the amount of fixed carbon. The data was analyzed using an element analyzer (Elementar Vario EL III). The oxygen content (wt/wt%) was determined using the method described below:

$$O\% = 100 - (C\% + N\% + H\%) \quad (1)$$

2.1 Production and characterization of activated biochar

In a fixed-bed reactor, 25 g of bagasse was loaded for physical activation. In an inert environment (i.e., N₂ gas was supplied at a flow rate of 1 L/min), the reactor temperature was raised from 27 to 600 °C at 10 °C/min. Nitrogen was substituted with CO₂ as the temperature reached 600 °C. CO₂ was supplied to the reactor with a flow rate of 2 L/min for 1 h. The reactor was cooled to normal temperature when the programme was completed. The biochar matrix’s closed pores can be opened and mixed with other pores to eliminate the majority of the carbonize precursors’ volatile carbon components [45]. A robust microporous structure with a low intensity of mesopores may therefore be seen in the physically activated biochar matrix, significantly increasing the specific surface area of the biochar.

Numerous experiments have been conducted to alter the characteristics of biochar using various activation agents in an effort to produce biochar with superior surface properties. Here, the term “modification” refers to the physical activation of the original biochar in order to accomplish the desired result. The surface area of biochar is influenced by the kind of activator, activation temperature, and activation period. Table 3 shows the surface area of the biochar after physical activation.

When CO₂ penetrated the top layer of the biochar, the pores expanded, increasing the surface area and quantity of adsorption-active sites. Adsorption capacity is significantly increased as a result of the additional functional groups that are present on the surface of the activated biochar bonding with other substances that serve as adsorption sites [13, 52]. According to the BET analysis, biochar’s surface area enhanced from 70.07 to 263.05 m²/g and pore volume from 0.082 to 0.159 cm³/g. Prior studies demonstrated that CO₂ activation enhanced surface area and churned out new porosities [53]. The following reactions took place (Table 4).

Table 2 Proximate and ultimate characteristics of bagasse

Feedstock	Proximate analysis (wt%)			Ultimate analysis (wt%)			
	VM	FC*	Ash	C	H	N	O*
Bagasse	72.48	22.65	1.37	48.77	7.384	0.849	42.99

FC, fixed carbon; VM, volatile matter; C, carbon; H, hydrogen; O, oxygen; *Calculated by the difference

Table 3 Literature of different activating agents' effect on surface area of biochar

Biomass	Activating agent	Activation temperature (°C)	Residence time (min)	Surface area (m ² /g)	Pore volume (cm ³ /g)	References
Aspen wood	CO ₂	800	20	540 (440)*	-	[46]
Oak	CO ₂	800	60	786 (107)*	0.337 (0.050)*	[47]
Giant Miscanthus	Steam	800	60	322 (181)*	-	[48]
Switchgrass	Steam	800	60	167.8 (3.62)*	-	[49]
Grape seed	O ₃	250	120	900 (47)*	0.04 (0.007)*	[50]
Douglas fir bark	Air	250	30	550 (424)*	0.81 (0.43)*	[51]
Woods of hybrid Popla	Air	250	30	570 (500)*	0.75 (0.57)*	[51]
ASB600	CO ₂	600	60	263.05 (70.07)*	0.159 (0.082)*	This work

*Surface area values before activation

Oxygen-containing molecules are produced when CO₂ interacts with biochar. The FTIR curve can confirm the surged presence of C=O, OH, and carboxyl groups at the surface.

The activated biochar obtained by CO₂ activation was labelled ASB600, and the non-activated biochar was labelled SB600. The mass ratio of biochar and activated biochar to feedstock was used to compute the yield, which is stated as follows:

$$\text{Yield \%} = \frac{\text{Weight of biochar / Activated biochar (kg)}}{\text{Weight of biomass (kg)}} \times 100 \quad (2)$$

2.2 Characterization

2.2.1 Fourier transform infrared (FTIR) analysis

The chemical functional groups contained in feedstock and biochar were determined via FTIR analysis. The study employed an FTIR spectrometer (Thermo Nicolet I5). The study was accomplished via the pellet approach, in which dried samples were mixed 1:10 (w/w) with dried KBr and then crushed under a vacuum to make pellets. Wavenumbers ranging from 4000 to 500 cm⁻¹ were used to generate absorption mode FTIR spectra.

2.2.2 Brunauer–Emmett–Teller (BET) analysis

Samples were pre-processed in a vacuum for 6 h at 200 °C before being put through a BET surface area test. The multi-point BET method was used to calculate specific surface areas.

2.2.3 Scanning electron microscope (SEM)

To analyze the surface morphology of biochar, an FEI Quanta 200F field emission SEM (FEI Company, Netherlands) was utilized. All trials were repeated thrice, and the average findings were provided.

2.3 pH and point of zero charge

A glass H⁺ electrode was dipped into the mixture just above the settled biochar to measure the pH after adding biochar to deionized water in a mixture with a 10:1 water to biochar (mL:g) ratio, letting the mixtures equilibrate for an hour.

The point at which the pH_{final} vs. pH_{initial} curve veers off from the pH_{final} = pH_{initial} line is known as the point of zero charge (pH_{PZC}). This procedure involved placing 50 mL of a 100 mg/L NAP aqueous solution in a 250 mL flask, adjusting the pH to a set value between 2 and 12 by adding 0.1 mol/L HCl or 0.1 mol/L NaOH solutions, and then adding 0.1 g of porous carbon to the solution in the flask while it was being shaken in a water bath at 25 °C. After 12 h, the pH was checked again to confirm equilibrium. The average of all the triplets in the experiment is provided.

2.4 PAH adsorption experiment

Batch adsorption equilibrium techniques were used to conduct the NAP adsorption experiment. The stock solutions of NAP (50 mg/L) were made utilizing ultrasound for 10 min at room temperature in a solution of 30% aqueous ethanol. The effectiveness of the biochar samples (SB600, ASB600) was tested by mixing 0.2 g of SB600 and 0.2 g of ASB600 with 50 mL of a solution containing 50 mg/L

Table 4 Chemical reaction involved during CO₂ activation

Oxidizing agent	Chemical reaction	Process	Reference
CO ₂	$C(\text{Char}) + \text{CO}_2 \rightarrow 2\text{CO}$	Carbon gasification by carbon dioxide	[54, 55]

of NAP, respectively, in a glass Erlenmeyer flask. The pH level was kept at 7 throughout each experiment. The solution’s pH was sustained at 7 by progressively adding 0.1 M of HCl or 0.1 M of NaOH solution. The samples were then shaken for a total of 240 min at a temperature of 25 °C, with intervals of 30, 60, 90, 120, 150, 180, and 210 min. The reaction mixture was stirred (140 rpm) while incubating. The samples were then filtered using the Whatman No. 1 filter. Spectrophotometer measurements were made of the NAP concentrations in the filtrate at the maximum absorption wavelength (219 nm). The adsorption experiments were conducted twice, and subsequent analysis was based on the average findings.

The adsorption capacities of NAP are given as Q_t (mg/g) at any time t ,

$$Q_t = (C_0 - C_t)V/m \tag{3}$$

C_0 and C_t (mg/L) are NAP initial and concentration at time t , respectively. V (L) is solution volume, and m (g) is biochar mass.

Pseudo-first-order (PFO) Eq. (4) and pseudo-second-order (PSO) Eq. (5), as narrated by Guo et al. [1] and Wu et al. [56], were used for the experiment to examine the mechanism of NAP adsorption onto biochar.

$$\text{Log}(q_e - q_t) = \text{Log}q_e - \frac{k_1 t}{2.303} \tag{4}$$

$$\frac{t}{q_t} = \frac{1}{k_2 q_e^2} + \frac{t}{q_e} \tag{5}$$

q_e and q_t (mg/g) are adsorbed quantities of NAP at equilibrium and time t (h), respectively, whereas k_1 (h^{-1}) and k_2 (g/mg·h) are rate constants for the kinetic models at equilibrium.

The maximum capacities of NAP adsorption by SB600 and ASB600 were estimated using the Langmuir (Eq. (6)) and Freundlich (Eq. (7)). The observations were carried out at room temperature (25 °C) using 0.2 g of SB600 and ASB600, 50 mL NAP solution, and NAP concentrations of 10, 20, 30, 40, 50, 80, 160, and 320 mg L^{-1} .

$$q = \frac{abC_e}{1 + bC_e} \tag{6}$$

$$q = KC_e^{\frac{1}{n}} \tag{7}$$

where q (mg/g) is NAP adsorbed, C_e (mg/L) is NAP equilibrium concentration, a is Langmuir constant, b is NAP binding strength, and K and $1/n$ are the Freundlich constants indicating the NAP adsorption capacity and intensity, respectively.

2.5 Thermodynamic analysis

Entropy (S°), enthalpy (H°), and Gibbs free energy (G°), three thermodynamic parameters, were calculated to determine how to process temperature impacts the NAP adsorption capacity of activated and non-activated biochar. As shown in Eqs. (8) and (9), the Van’t Hoff equation was used to determine the thermodynamic parameters [57].

$$\Delta G^\circ = -RT \ln K_t \tag{8}$$

$$\ln K_t = \frac{\Delta S^\circ}{R} - \frac{\Delta H^\circ}{RT} \tag{9}$$

3 Results and discussion

3.1 Characterization of biochar

The biochar yield for SB600 (non-activated biochar) and ASB600 (activated biochar) was obtained 24.31% and 11.09%, respectively, as mentioned in Table 5.

The N_2 adsorption–desorption investigation was used to examine the SSA (specific surface area) and porosity of the SB600 and ASB600. The pore characteristics of all the samples are detailed in Table 5. The surface area of the SB600 was more than that of the raw material (70.07 m^2/g). But the level remained low. The SSA and pore volume dramatically increased after pyrolysis, while the average pore width was reduced to 2.33 nm. The SSA of SB600 was shown to have expanded considerably by more than 17.9 times, going to 70.07 m^2/g from 3.91 m^2/g . The SSA of ASB600 is 263.05 m^2/g , which is over 3.5 times greater than SB600. The total pore volume of the SB600 rose by about 12 times, from 0.0067 to 0.082 cm^3/g , whereas the total pore volume of the ASB600 increased by 23 times, to 0.159 cm^3/g . Bagasse

Table 5 Biochar yield, surface area, pH, and pH_{pZC}

Material	Specific surface area (m^2/g)	Average pore size (nm)	Total pore volume (cm^3/g)	Biochar yield (%)	pH	pH_{pZC}
Bagasse	3.91	24.86	0.0067	-	4.3	4.21
SB600	70.07	2.53	0.082	24.31	7.58	6.42
ASB600	263.05	1.94	0.159	11.09	8.40	7.03

contains exceedingly small mesopores (24.86 nm) and has a limited pore size range. Most of the pores in SB600 and ASB600 had pore diameters of 2.33 nm and 1.94 nm, respectively. These findings enhanced the adsorbent's potential for sorption by demonstrating considerable activation and an abundance of microporous structure.

Additionally, the pore volume of the SB600 rose by about 12 times, reaching $0.082 \text{ cm}^3/\text{g}$ from $0.0067 \text{ cm}^3/\text{g}$, while the total pore volume of the ASB600 increased by 23 times to $0.159 \text{ cm}^3/\text{g}$. Mesopores in bagasse are extremely small (24.86 nm), and the range of pore diameters is constrained. Micropores comprise most of SB600 and ASB600's pores, with pore sizes of 2.33 nm and 1.94 nm, respectively. These results, which showed a high activation level and a significant amount of microporous structure, increased the adsorbent's capacity for adsorption.

The adsorbent's high surface area and large pore volume imply an improvement in the sorption capacity of organic contaminants such as the PAHs, which is caused by the pore-filling activity [58, 59]. Furthermore, the point of zero charge (pH_{pzc}) measured for SB600 is 6.42 and for ASB600 is 7.03 (Table 5). The pH of the solution may be easily altered to be higher than the pH at the PZC, and the SB600 and ASB600 showed lower PZC values, making them compatible with cationic aromatic hydrocarbons like NAP. The negatively charged surface of the biochar facilitates the adsorption of cations when $\text{pH} > \text{pH}_{\text{PZC}}$.

3.2 FTIR analysis

The FTIR spectra of bagasse (SB), SB600, and ASB600 in the $4000\text{--}500 \text{ cm}^{-1}$ wavenumber region are demonstrated in Fig. 1. Because there is lignin and carbohydrates present, the peak between 3410 and 3300 cm^{-1} is the result of intermolecular O–H stretching hydrogen bonding [60] (Fig. 1). The peak at 3410 cm^{-1} of SB falls when pyrolysis and activation take place. During pyrolysis, the hydroxyl group in the biomass structure contracts, resulting in significant carbonization. In addition to C–H asymmetric and symmetric stretching, the peak at 2924 cm^{-1} is attributed to C–H aliphatic axial deformation in CH_2 and CH_3 groups from cellulose, lignin, and hemicellulose. The peak softens during pyrolysis and activation due to the solid waste's carbonization. Hemicellulose makes the broad band at 1730 cm^{-1} , a feature of the carbonyl band, and is induced by the C=O stretching vibration present. Heat is used to degrade the three main constituents of lignocellulosic biomass, and carbonyl is one of the intermediate chemicals created in each case [41, 42, 54]. After the pyrolysis reaction processes are complete, these intermediate products undergo further degradation, which reduces the 1730 cm^{-1} C=O stretching peak on the SB600 and ASB600 spectrum. The SB600 and ASB600 spectra still clearly show the 1730 cm^{-1} stretching

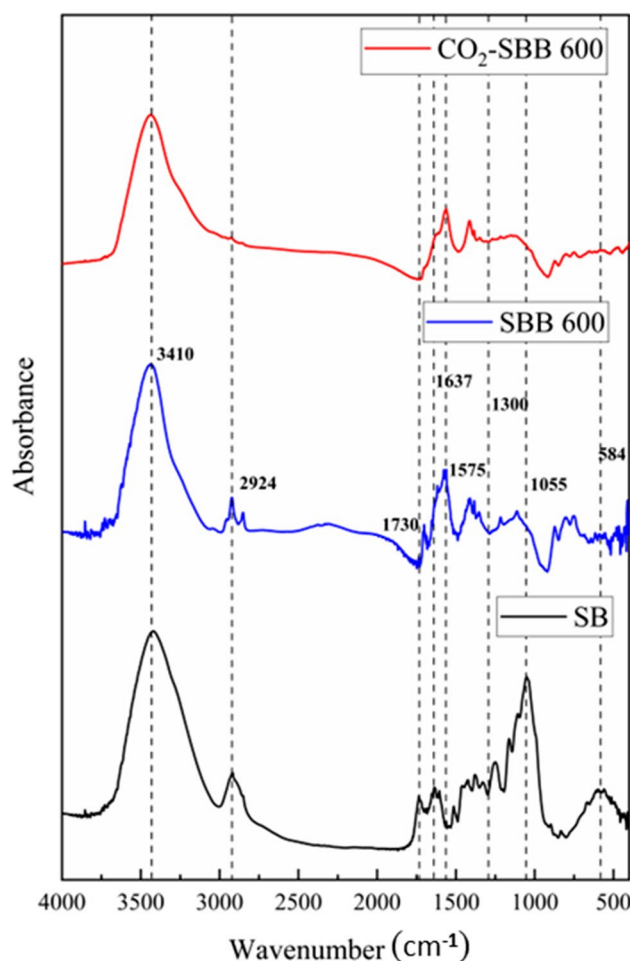


Fig. 1 FTIR spectra of bagasse, non-activated, and activated biochar

peak. Due to the presence of lignin, peaks between 1700 and 1500 cm^{-1} are suggestive of the C=C aromatic ring and an O–H phenolic hydroxyl group. Lignin contributes significantly to the C=C stretching of aromatic substances peak at around 1500 cm^{-1} in the Luffa spectrum because it is the only substantial aromatic component of lignocellulosic biomass. Furfural, hydroxymethylfurfural, and other aromatic heterocyclic compounds known as furanoses are produced when cellulose is broken down by heat [42]. The degradation of lignin and the thermal decomposition of furanoses both reduce this peak on ASB600 spectra. The peak for C=C stretching of aromatic compounds is still visible in ASB600 spectra, indicating that lignin has been retained and subsequent pyrolysis has only occurred to a lesser extent. As the temperature rises, bagasse degradation and product volatilization cause peaks between 1500 and 1300 cm^{-1} to decrease. Since hemicelluloses have already been disintegrated in both non-activated and activated biochar, the C–O–C stretching peak, which is connected to the glycosidic bond of the hemicelluloses, is only present in the bagasse spectrum. It

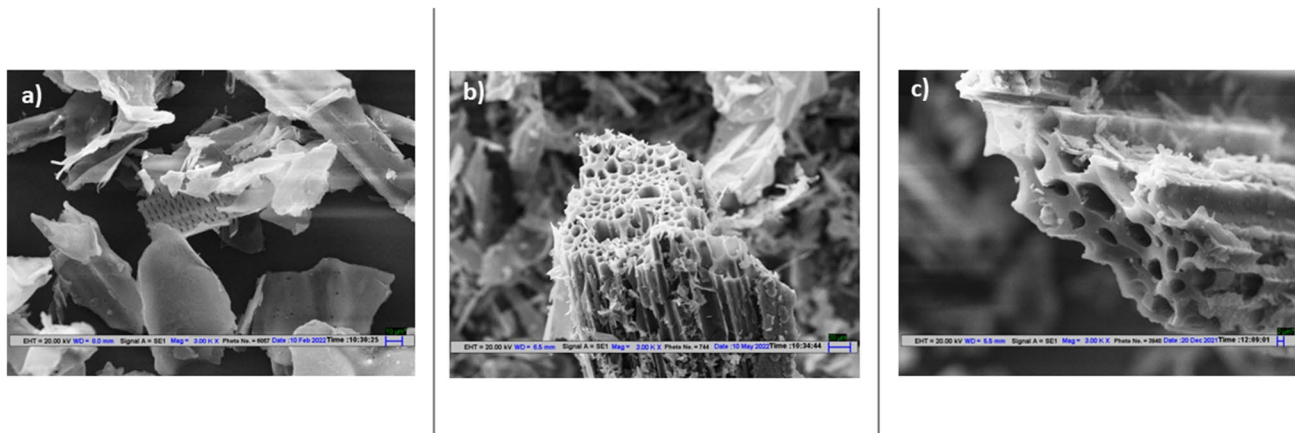


Fig. 2 SEM images of **a** bagasse, **b** SB600, and **c** ASB600

is plausible that the activation step was successful in creating surface functional groups with oxygen since activated biochar has more C=O groups than raw biochar.

3.3 SEM analysis

All three samples underwent SEM examination (Fig. 2). According to the SEM images, the bagasse has a few microscopic holes and indentations but no channels, fissures, or porous features. A few pores, created during pyrolysis, were present on the bagasse's surface. The CO₂ activation was effective in developing well-developed pores and biochar's surface. During activation, CO₂ penetrated the biochar matrix's internal pore structure and gasified the carbon molecules there, which led to previously inaccessible pores opening and enlarging [61]. The illustration in Fig. 2 made it quite clear how the

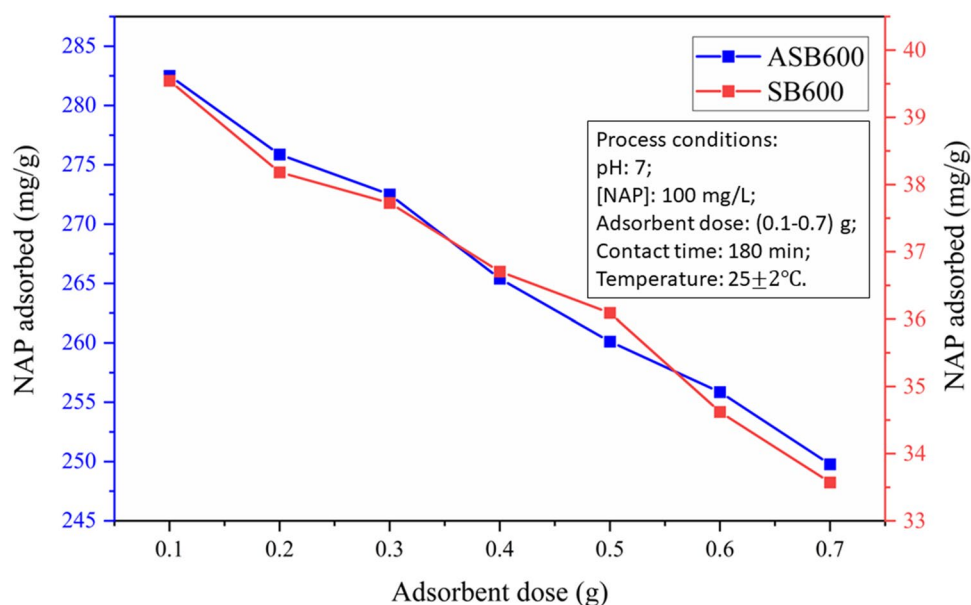
physical activation changed the surface's morphology. As a result, it was discovered that ASB600's surface was uneven and rough. Since the activation impact is so strong, ASB600 has more microporous structures than SB600. High porosity ASB600 is a better option for use as an adsorbent.

3.4 NAP adsorption studies

3.4.1 Effect of adsorbent dose

The results of the adsorption experiment with various doses of ASB600 and SB600 (0.1–0.7 g) are shown in Fig. 3. The findings show that as adsorbent dosage is increased, NAP adsorption decreases. After 0.1 g, the NAP adsorption capacity declines as the adsorbent dose rises; this can be due to problems with aggregation brought on by high

Fig. 3 Effect adsorbent dosage on NAP adsorption



adsorbent dosage. As a result, the diffusional path length was enhanced while the binding sites and adsorbent surface area were decreased [62, 63].

3.4.2 Effect of contact time and adsorption kinetics

A solution of NAP-containing adsorbent was mechanically shaken for varied time intervals (10–240 min) in order to examine the impact of contact time on the adsorption of NAP on ASB600 and SB600. For ASB600, adsorption increased for 120 min, whereas for SB600, adsorption increased for 180 min before being constant (Fig. 4). An average shaking time of 180 min was noted for all following investigations. The adsorption was examined to ensure that prolonged shaking had no negative effects.

The adsorbent surface's abundance of surface functional groups and pores during the initial stages of adsorption provided more adsorption sites. As a result, ions bond to the adsorbent surface with ease. As the process of adsorption advanced, active adsorption sites gradually decreased, and the rate of adsorption slowed until adsorption equilibrium was reached. This is because as adsorbent molecules filled the active sites, physical constraints and repulsive forces made it harder for vacant sites to be contacted. The results showed that ASB600 was more effective in removing NAP and had a larger adsorption capacity (290.43 mg/g vs. SB600's 38.15 mg/g). This might be brought on by the greater surface area, surface pores, and surface functioning of activated biochar. The kinetic adsorption results demonstrated that the pseudo-second-order model's R^2 (0.99) was

more developed in NAP adsorption than the pseudo-first-order model's R^2 (0.95) (Fig. 5) (Table 6). The former was found to be the most suitable explanation for the adsorption kinetics of ASB600 and SB600 NAP. Regarding the chemisorption mechanism, which constrained chemical sorption by transferring electrons between divalent metal ions and polar surface functional groups of biochar, the PSO model performed well for adsorption.

3.4.3 Adsorption isotherms

As shown in Fig. 6, the quantity of NAP adsorbed on the SB600 and ASB600 increased as the initial NAP concentration increased, eventually reaching the optimum adsorption limit. It might be owing to the limited number of adsorption sites on the biochar surface [39]. As the NAP concentration rose, the majority of active sites were occupied, making it challenging for the adsorbate to utilize the remaining active sites. The Langmuir and Freundlich models provided good fits to the sorption data (Table 7). For ASB600, the Langmuir model ($R^2 > 0.97$) was more appropriate since it showed that the majority of adsorption was monolayer, which may encompass both physical and chemical sorption. The Freundlich model ($R^2 = 0.98$ for SB600) fit more accurately for non-activated biochar, which shows multi-layer adsorption of non-uniform surfaces. The isothermal curve's Freundlich constant was $1/n < 1$, showing that the adsorption isotherm was of the L type. Its value ranged from 0.1 to 0.5, indicating that

Fig. 4 Effect of contact time on NAP adsorption

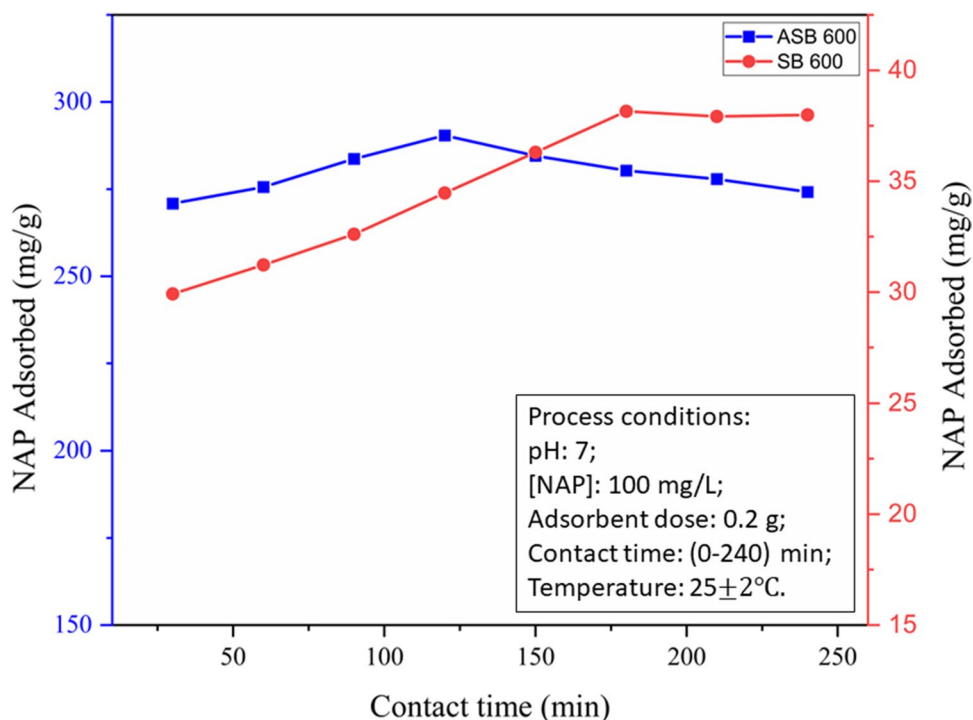


Fig. 5 Pseudo-first- and second-order fit for ASB600

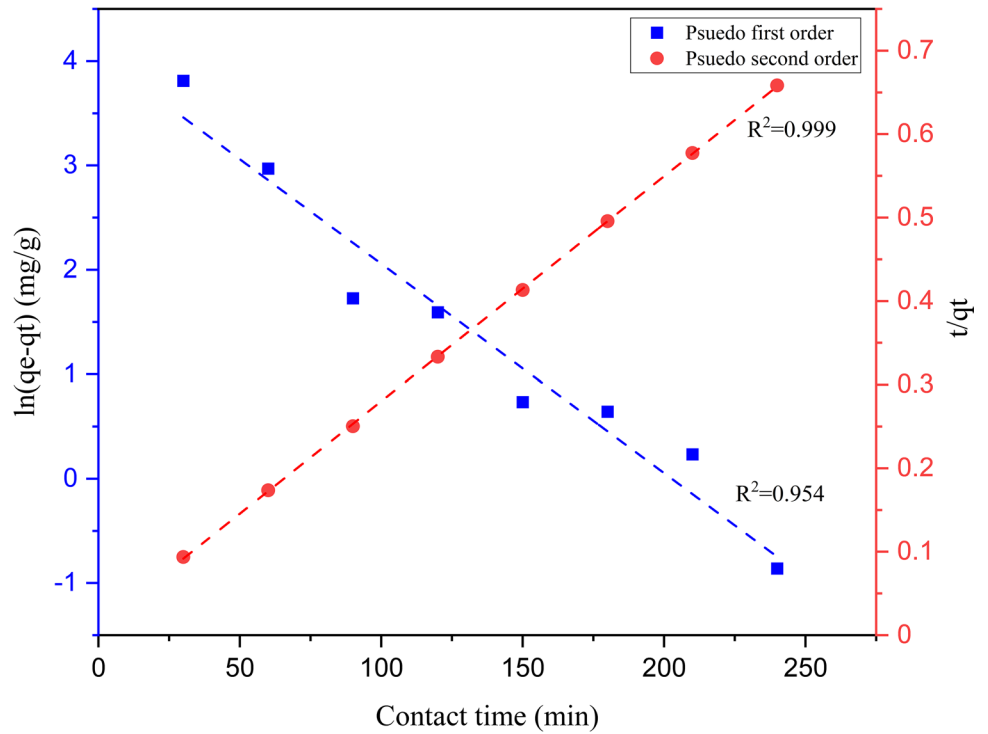


Table 6 Adsorption kinetics

Adsorbent	PFO			PSO		
	q_e	K_1	R^2	q_e	K_2	R^2
ASB600	2.15	0.020	0.95	292.01	0.0017	> 0.99
SB600	1.541	0.025	0.93	40.81	0.0014	> 0.99

Fig. 6 Effect of initial NAP concentration on NAP adsorption

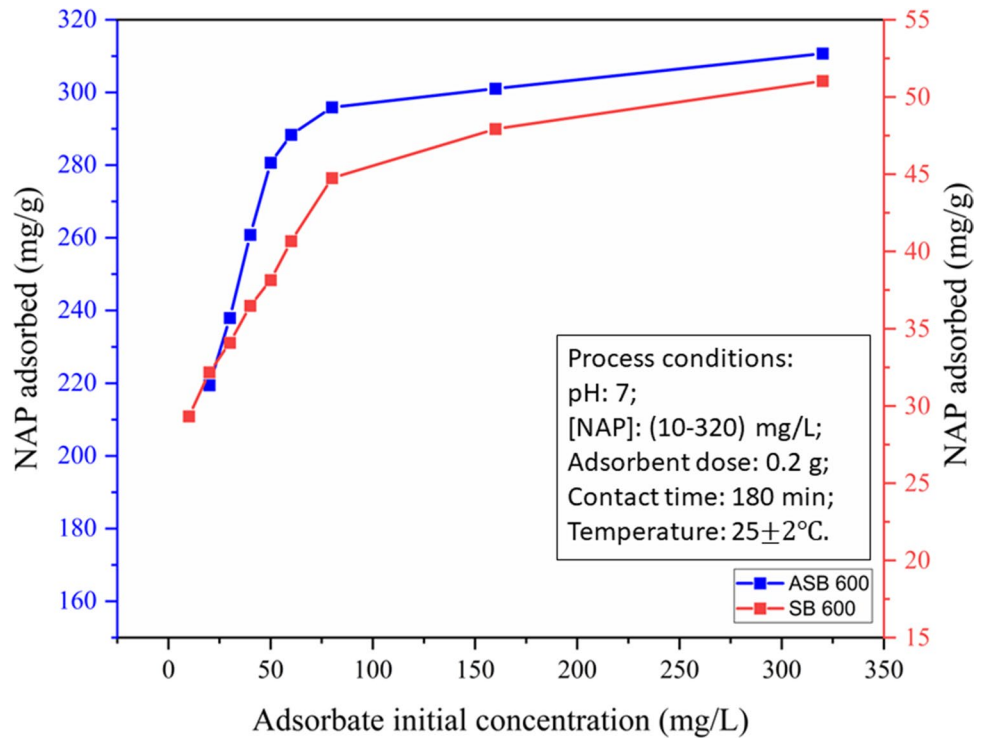


Table 7 Adsorption isotherms

Adsorbent	Langmuir			Freundlich		
	q_{\max}	K_L	R^2	$1/n$	K_2	R^2
ASB600	312.5	2.205	0.97	0.6257	9.26	0.86
SBB600	44.05	1.76	0.80	0.3909	1.143	0.98

naphthalene adsorption on the surfaces of SB600 was simple.

3.4.4 Adsorption mechanism

Several methods are given for comprehending the adsorption mechanism of aromatic compounds. According to results of experiments, interaction between the electrons in the benzene ring of the adsorbate and the electrons distributed on the carbon surface stimulates the adsorption process. The literature claims that the acidic pH encourages aromatic molecules to align themselves with the surface of AC, specifically from the edges to the face at various tilt angles. There may be other research using similar methods to describe the adsorbate-adsorbent interaction via the electrostatic interaction [64].

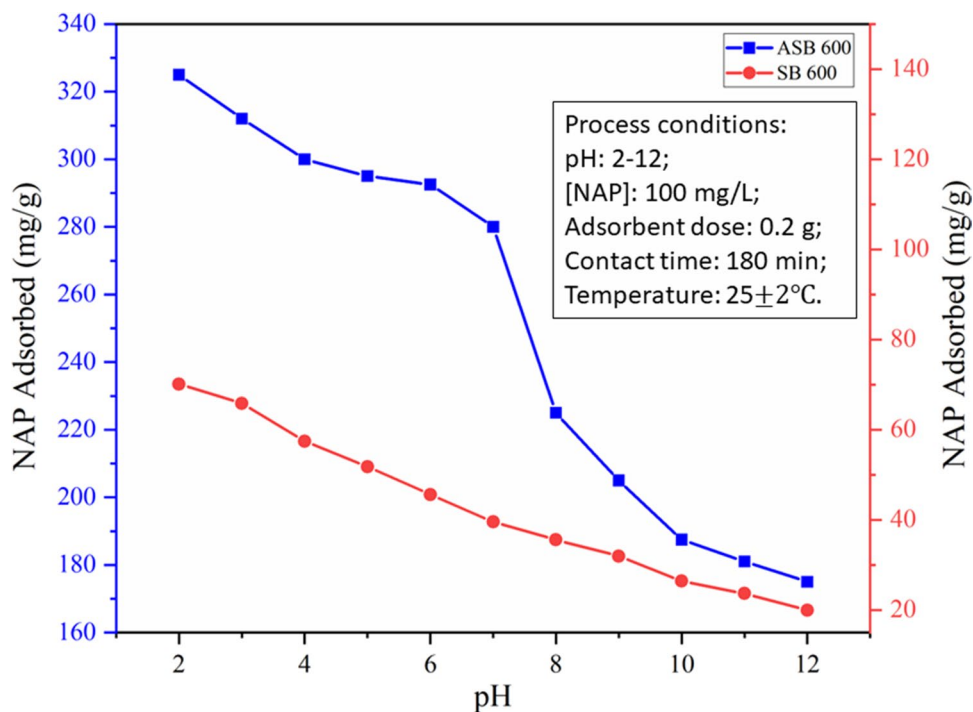
3.4.5 Hydrogen bonds

Hydrogen bonds may also form between the adsorbent and the molecules of the adsorbate when they have specific functional groups, such as -COOH and -OH [65]. The ASB600 and SB600 FTIR spectra in Fig. 1 demonstrate the presence

of the -OH and C=O groups. Given that NAP molecules include -OH groups, hydrogen bonding between NAP and adsorbent is possible. The following facts imply that the high adsorption capacity was not primarily caused by hydrogen bonding. One is that there are not enough functional groups in adsorbents to serve as a reliable hydrogen-bonding donor [66, 67]. The second is that the hydrogen bonding interaction between molecules of water and functional groups on an adsorbent's surface is substantially higher than that between aromatic compounds and functional groups [67].

3.4.6 Electrostatic interactions

The interpretation of the adsorption of aromatic chemicals onto ASB600 and SB600 has also been achieved using molecular electrostatic attraction [68]. In the pH range of 2 to 12, the impact of pH on the adsorption of NAP onto activated and non-activated biochar was examined. The results are displayed in Fig. 7, which demonstrates that NAP adsorption declines as pH increases. The findings further imply that greater electrostatic interactions between the positively charged adsorbent surface and PAH, which account for enhanced adsorption, are present at low pH and that this

Fig. 7 Effect of solution's pH on NAP adsorption

positive charge on the adsorbent’s surface contributes to the increased PAH adsorption at low pH. The adsorption of PAHs decreases with pH as a result of a decrease in surface positive charge, which is followed by a decline in the electrostatic attraction between the adsorbate and adsorbent. Competition between OH ions increases as pH rises.

Table 8 summarizes the various biochars for NAP adsorptions. Although the adsorption capacity for SB600 found in this investigation was less than certain reported values in the literature, it was occasionally higher or at least on par with the adsorption capacities of other lignocellulosic biomasses. However, the adsorption capacity of ASB600 was greater than most reported values in literature, with the exception of one (the biochar produced in that study was chemically activated and thus having higher surface area). Even while ASB600 has a lower maximum adsorption value (q_e) than chemically activated carbon made from bean pods [69], this difference is nonetheless advantageous because the chemical compounds employed in chemical activation are not eco-friendly and are damaging to the research equipment [70]. Additionally, after the adsorbent reaches saturation, it can be used in cogeneration to provide electricity to the sector [71]. These qualities make biochar made from bagasse more cost-effective than other low-cost adsorbents.

3.4.7 Thermodynamic analysis

Studies were conducted at various adsorption temperatures (20, 30, 40, and 50 °C) to determine how temperature and thermodynamic analyses of NAP adsorption on ASB600 and SB600 affected the results. The adsorption process was positively affected with the rise in temperature (Table 9). NAP adsorption on both the biochar and higher

temperatures was shown to be an endothermic process since the change in enthalpy at these temperatures was positive. The values of 11.03 and 10.004 kJ/kg, respectively, for ASB600 and SB600 were determined. Higher value of H° during NAP adsorption by ASB600 as compared to SB600 suggests a more solid bond between the NAP molecule and the active site.

Entropy changes (S°) due to adsorption by ASB600 and SBB600 were 11.03 and 10.004 kJ/mol K, respectively. The increased system disorder is implied by the positive value of S° , which shows that irreversibility of adsorption mechanism. The adsorption process is thermodynamically viable and spontaneous based on the negative value of G° . Due to reduced electron transport, molecular heat generation, and mass transfer between the adsorbent and adsorbate at the interface layer, low temperatures make NAP mass transfer difficult. As the process temperature increased, the NAP molecule’s intensity and frequency of interactions with the

Table 9 Thermodynamic parameters

Material	Temperature (K)	ΔH° (kJ/mol)	ΔS° (kJ/mol K)	ΔG° (kJ/mol)
ASB600	293	11.03	40.84	- 1.92
	303			- 2.24
	313			- 2.68
	323			- 3.14
SBB600	293	10.004	40.58	- 0.87
	303			- 1.42
	313			- 1.77
	323			- 2.11

Table 8 Comparison of adsorption capacities of various agro residues for different organic pollutants

Biochar	Pollutant	Adsorbent dose	pH	Contact time (hour)	PAH initial concentration (mg/L)	Adsorption capacity/ Reference removal efficiency
AC	NAP	50 mg	-	-	30	15.41 mg/g [3]
AG-5 AC	NAP	-	5–7	2	-	24.57 mg/g [72]
DTO AC	NAP	-	5–7	2	-	30.28 mg/g [72]
Pine wood	NAP	50 mg	-	15	23.7	208 mg/g [73]
Unripe orange peel	NAP	7.5 g	6	3	100	90% [74]
Wheat straw AC	NAP	0.2 g	7	2	32	69.6 mg/g [38]
Rice husk AC	NAP	2 mg	-	24	8	63.6 mg/g [75]
Bean pods AC	NAP	40	5.5	72	30	300 mg/g [69]
SBAC	Phenol	0.2 g	-	4	100	24.68 mg/g [76]
SB pith AC	Reactive dye	5 g	1	2	20	3.92 mg/g [77]
SBAC	Petroleum hydrocarbon	10 g	4.5	3	5	8.36 mg/g [78]
SB	Methylene blue	2 g	-	3	5	4.41 mg/g [79]
SB600	NAP	2	7	3	100	38.15 mg/g This work
ASB600	NAP	2	7	2	100	290.5 mg/g This work

biochar surface in the solution increased noticeably, improving adsorption performance. Similar outcomes were reported for the adsorption of basic dyes and tartrazine [80, 81].

4 Conclusion

Utilizing activated bagasse in a single step, naphthalene from an aqueous solution was adsorbed. Compared to non-activated biochar, CO₂-activated biochar has a finer granular, porous structure with a bigger surface area. According to the FTIR measurement, biochar has hydroxyl and carbonyl groups, which have a greater capability for adsorption. Activated carbon has a higher naphthalene adsorption capacity than non-activated biochar (290.5 mg/g vs. 38.15 mg/g). The pseudo-second-order and Langmuir models were applied in accordance with the adsorption kinetics and isotherms for activated biochar. Adsorption was endothermic, spontaneous, and temperature increase-favorable according to the thermodynamic characteristics.

Acknowledgements The authors would like to thank the Centre for Rural Development and Technology (CRDT) Indian Institute of Technology (IIT) Delhi and the Prime Minister's Research Fellowship programme of GoI for carrying out the work.

Author contribution SP: conceptualization, data curation, writing original draft, editing.

KKP: review and resources.

PK: research facilitation, review, and overall supervision.

We confirm that the manuscript has been read and approved by all named authors and that there are no other persons who satisfied the criteria for authorship but are not listed. We confirm that all have approved the order of authors listed in the manuscript.

Data availability Not applicable.

Declarations

Ethics approval Not applicable.

Competing interests The authors declare no competing interests.

References

1. Shaarani FW, Hameed BH (2011) Ammonia-modified activated carbon for the adsorption of 2,4-dichlorophenol. *Chem Eng J* 169:180–185. <https://doi.org/10.1016/J.CEJ.2011.03.002>
2. Liu QS, Zheng T, Li N et al (2010) Modification of bamboo-based activated carbon using microwave radiation and its effects on the adsorption of methylene blue. *Appl Surf Sci* 256:3309–3315. <https://doi.org/10.1016/J.APSUSC.2009.12.025>
3. Cabal B, Ania CO, Parra JB, Pis JJ (2009) Kinetics of naphthalene adsorption on an activated carbon: comparison between aqueous and organic media. *Chemosphere* 76:433–438. <https://doi.org/10.1016/J.CHEMOSPHERE.2009.04.002>
4. Vassileva P, Tzvetkova P, Nickolov R (2009) Removal of ammonium ions from aqueous solutions with coal-based activated carbons modified by oxidation. *Fuel* 88:387–390. <https://doi.org/10.1016/J.FUEL.2008.08.016>
5. Yin CY, Aroua MK, Daud WMAW (2007) Review of modifications of activated carbon for enhancing contaminant uptakes from aqueous solutions. *Sep Purif Technol* 52:403–415. <https://doi.org/10.1016/J.SEPPUR.2006.06.009>
6. Tan IAW, Ahmad AL, Hameed BH (2008) Enhancement of basic dye adsorption uptake from aqueous solutions using chemically modified oil palm shell activated carbon. *Colloids Surf A Physicochem Eng Asp* 318:88–96. <https://doi.org/10.1016/J.COLSURFA.2007.12.018>
7. Zhang Z, Xu M, Wang H, Li Z (2010) Enhancement of CO₂ adsorption on high surface area activated carbon modified by N₂, H₂ and ammonia. *Chem Eng J* 160:571–577. <https://doi.org/10.1016/J.CEJ.2010.03.070>
8. Karam FF, Hussein FH, Baqir SJ et al (2014) Photocatalytic degradation of anthracene in closed system reactor. *Int J Photoenergy* 2014:1–7. <https://doi.org/10.1155/2014/503825>
9. Silva MJ, Soares SAR, Santos IDF et al (2020) Optimization of the photocatalytic degradation process of aromatic organic compounds applied to mangrove sediment. *Heliyon* 6:e05163. <https://doi.org/10.1016/j.heliyon.2020.e05163>
10. Smol M, Włodarczyk-Makuła M, Mielczarek K et al (2016) The use of reverse osmosis in the removal of PAHs from municipal landfill leachate. *Polycycl Aromat Compd* 36:20–39. <https://doi.org/10.1080/10406638.2014.957403>
11. Sakhiya AK, Anand A, Kaushal P (2020) Production, activation, and applications of biochar in recent times. Springer, Singapore
12. Franciski MA, Peres EC, Godinho M et al (2018) Development of CO₂ activated biochar from solid wastes of a beer industry and its application for methylene blue adsorption. *Waste Manage* 78:630–638. <https://doi.org/10.1016/j.wasman.2018.06.040>
13. Ademiluyi FT, David-West EO (2012) Effect of chemical activation on the adsorption of heavy metals using activated carbons from waste materials. *ISRN Chemical Engineering* 2012:1–5. <https://doi.org/10.5402/2012/674209>
14. Sakhiya AK, Baghel P, Anand A et al (2021) A comparative study of physical and chemical activation of rice straw derived biochar to enhance Zn²⁺ adsorption. *Bioresour Technol Rep* 15:100774. <https://doi.org/10.1016/J.BITEB.2021.100774>
15. Lamichhane S, Bal Krishna KC, Sarukkalige R (2016) Polycyclic aromatic hydrocarbons (PAHs) removal by sorption: a review. *Chemosphere* 148:336–353. <https://doi.org/10.1016/j.chemosphere.2016.01.036>
16. Boving TB, Zhang W (2004) Removal of aqueous-phase polynuclear aromatic hydrocarbons using aspen wood fibers. *Chemosphere* 54:831–839. <https://doi.org/10.1016/j.chemosphere.2003.07.007>
17. Bojes HK, Pope PG (2007) Characterization of EPA's 16 priority pollutant polycyclic aromatic hydrocarbons (PAHs) in tank bottom solids and associated contaminated soils at oil exploration and production sites in Texas. *Regul Toxicol Pharmacol* 47:288–295. <https://doi.org/10.1016/j.yrtph.2006.11.007>
18. Fernandes A, Rose M, Falandysz J (2017) Polychlorinated naphthalenes (PCNs) in food and humans. *Environ Int* 104:1–13. <https://doi.org/10.1016/j.envint.2017.02.015>
19. Dai Y, Niu J, Yin L et al (2013) Laccase-carrying electrospun fibrous membrane for the removal of polycyclic aromatic hydrocarbons from contaminated water. *Sep Purif Technol* 104:1–8. <https://doi.org/10.1016/J.SEPPUR.2012.11.013>
20. Zhu L, Li S, Hu T et al (2019) Effects of nitrogen source heterogeneity on nutrient removal and biodiesel production of mono- and mix-cultured microalgae. *Energy Convers Manag* 201:112144. <https://doi.org/10.1016/J.ENCONMAN.2019.112144>
21. Liao X, Wu Z, Li Y et al (2018) Enhanced degradation of polycyclic aromatic hydrocarbons by indigenous microbes combined

- with chemical oxidation. *Chemosphere* 213:551–558. <https://doi.org/10.1016/j.chemosphere.2018.09.092>
22. Dowaidar AM, El-Shahawi MS, Ashour I (2007) Adsorption of polycyclic aromatic hydrocarbons onto activated carbon from non-aqueous media: 1. The influence of the organic solvent polarity. *Sep Sci Technol* 42:3609–3622. <https://doi.org/10.1080/01496390701626537>
 23. Guieysse B, Viklund G, Toes AC, Mattiasson B (2004) Combined UV-biological degradation of PAHs. *Chemosphere* 55:1493–1499. <https://doi.org/10.1016/J.CHEMOSPHERE.2004.01.021>
 24. Wu M, Pan B, Zhang D et al (2013) The sorption of organic contaminants on biochars derived from sediments with high organic carbon content. *Chemosphere* 90:782–788. <https://doi.org/10.1016/J.CHEMOSPHERE.2012.09.075>
 25. Nowacka A, Włodarczyk-Makuløa M (2015) Effectiveness of priority PAH removal in a water coagulation process. *Water Sci Technol Water Supply* 15:683–692. <https://doi.org/10.2166/ws.2015.023>
 26. Shabeer TPA, Saha A, Gajbhiye VT et al (2014) Removal of poly aromatic hydrocarbons (PAHs) from water: effect of nano and modified nano-clays as a flocculation aid and adsorbent in coagulation-flocculation process. *Polycycl Aromat Compd* 34:452–467. <https://doi.org/10.1080/10406638.2014.895949>
 27. Nyström F, Nordqvist K, Herrmann I, et al (2020) Removal of metals and hydrocarbons from stormwater using coagulation and flocculation. *Water Res* 182. <https://doi.org/10.1016/j.watres.2020.115919>
 28. Bisht S, Pandey P, Bhargava B et al (2015) Bioremediation of polyaromatic hydrocarbons (PAHs) using rhizosphere technology. *Braz J Microbiol* 46:7–21. <https://doi.org/10.1590/S1517-838246120131354>
 29. Gupte A, Tripathi A, Patel H et al (2016) Bioremediation of polycyclic aromatic hydrocarbon (PAHs): a perspective. *Open Biotechnol J* 10:363–378. <https://doi.org/10.2174/1874070701610010363>
 30. Egli SN, Butler ED, Bottaro CS (2015) Selective extraction of light polycyclic aromatic hydrocarbons in environmental water samples with pseudo-template thin-film molecularly imprinted polymers. *Anal Methods* 7:2028–2035. <https://doi.org/10.1039/c4ay02849j>
 31. Adeola AO, Forbes PBC (2021) Advances in water treatment technologies for removal of polycyclic aromatic hydrocarbons: existing concepts, emerging trends, and future prospects. *Water Environ Res* 93:343–359. <https://doi.org/10.1002/wer.1420>
 32. Lee PH, Ong SK, Golchin J, Nelson GL (1999) Extraction method for analysis of PAHs in coal-tar-contaminated soils. *Pract Period Hazard, Toxic, Radioact Waste Manag* 3:155–162. [https://doi.org/10.1061/\(ASCE\)1090-025X\(1999\)3:4\(155\)](https://doi.org/10.1061/(ASCE)1090-025X(1999)3:4(155))
 33. Von Lau E, Gan S, Ng HK, Poh PE (2014) Extraction agents for the removal of polycyclic aromatic hydrocarbons (PAHs) from soil in soil washing technologies. *Environ Pollut* 184:640–649. <https://doi.org/10.1016/j.envpol.2013.09.010>
 34. Chen F, Hong M, You W et al (2015) Simultaneous efficient adsorption of Pb²⁺ and MnO₄⁻ ions by MCM-41 functionalized with amine and nitrilotriacetic acid anhydride. *Appl Surf Sci* 357:856–865. <https://doi.org/10.1016/j.apsusc.2015.09.069>
 35. Haneef T, Ul Mustafa MR, Yusof KW et al (2020) Removal of polycyclic aromatic hydrocarbons (PAHs) from produced water by ferrate (VI) oxidation. *Water (Switzerland)* 12:1–17. <https://doi.org/10.3390/w12113132>
 36. Qiao J, Xiong Y (2021) Electrochemical oxidation technology: a review of its application in high-efficiency treatment of wastewater containing persistent organic pollutants. *J Water Process Eng* 44:102308. <https://doi.org/10.1016/j.jwpe.2021.102308>
 37. Yin Z, Liu Y, Liu S et al (2018) Activated magnetic biochar by one-step synthesis: enhanced adsorption and coadsorption for 17 β -estradiol and copper. *Sci Total Environ* 639:1530–1542. <https://doi.org/10.1016/J.SCITOTENV.2018.05.130>
 38. Jiang YF, Hu XF, Yves U (2014) Effectiveness and mechanisms of Naphthalene Adsorption by biochar pyrolyzed from wheat straw. *Adv Environ Res*
 39. Rinawati, Hidayat D, Supriyanto R, et al (2019) Adsorption of polycyclic aromatic hydrocarbons using low-cost activated carbon derived from rice husk. *J Phys Conf Ser* 1338. <https://doi.org/10.1088/1742-6596/1338/1/012005>
 40. CECO CECO Mefiag-CECO Mefiag-Filter Media-Activated Carbon. <https://www.environmental-expert.com/products/ceco-mefiag-activated-carbon-filter-tubes-638430>. Accessed 10 May 2021
 41. Yaashikaa PR, Kumar PS, Varjani S, Saravanan A (2020) A critical review on the biochar production techniques, characterization, stability and applications for circular bioeconomy. *Biotechnol Rep* 28:e00570. <https://doi.org/10.1016/J.BTRE.2020.E00570>
 42. Liu G, Niu Z, Van Niekerk D et al (2008) Polycyclic aromatic hydrocarbons (PAHs) from coal combustion: emissions, analysis, and toxicology. *Rev Environ Contam Toxicol* 192:1–28. https://doi.org/10.1007/978-0-387-71724-1_1
 43. Zheng H, Wang Z, Deng X et al (2013) Characteristics and nutrient values of biochars produced from giant reed at different temperatures. *Bioresour Technol* 130:463–471. <https://doi.org/10.1016/J.BIORTECH.2012.12.044>
 44. Park J, Hung I, Gan Z et al (2013) Activated carbon from biochar: influence of its physicochemical properties on the sorption characteristics of phenanthrene. *Bioresour Technol* 149:383–389. <https://doi.org/10.1016/j.biortech.2013.09.085>
 45. Liu N, Charrua AB, Weng CH et al (2015) Characterization of biochars derived from agricultural wastes and their adsorptive removal of atrazine from aqueous solution: a comparative study. *Bioresour Technol* 198:55–62. <https://doi.org/10.1016/J.BIORTECH.2015.08.129>
 46. Veksha A, Bhuiyan TI, Hill JM (2016) Activation of aspen wood with carbon dioxide and phosphoric acid for removal of total organic carbon from oil sands produced water: increasing the yield with bio-oil recycling. *Materials* 9. <https://doi.org/10.3390/ma9010020>
 47. Jung SH, Kim JS (2014) Production of biochars by intermediate pyrolysis and activated carbons from oak by three activation methods using CO₂. *J Anal Appl Pyrolysis* 107:116–122. <https://doi.org/10.1016/j.jaap.2014.02.011>
 48. Shim T, Yoo J, Ryu C et al (2015) Effect of steam activation of biochar produced from a giant Miscanthus on copper sorption and toxicity. *Bioresour Technol* 197:85–90. <https://doi.org/10.1016/j.biortech.2015.08.055>
 49. Han Y, Boateng AA, Qi PX et al (2013) Heavy metal and phenol adsorptive properties of biochars from pyrolyzed switchgrass and woody biomass in correlation with surface properties. *J Environ Manage* 118:196–204. <https://doi.org/10.1016/j.jenvman.2013.01.001>
 50. Jimenez-Cordero D, Heras F, Alonso-Morales N et al (2015) Ozone as oxidation agent in cyclic activation of biochar. *Fuel Process Technol* 139:42–48. <https://doi.org/10.1016/j.fuproc.2015.08.016>
 51. Suliman W, Harsh JB, Abu-Lail NI et al (2016) Modification of biochar surface by air oxidation: role of pyrolysis temperature. *Biomass Bioenergy* 85:1–11. <https://doi.org/10.1016/J.BIOMBIOE.2015.11.030>
 52. Tee GT, Gok XY, Yong WF (2022) Adsorption of pollutants in wastewater via biosorbents, nanoparticles and magnetic biosorbents: a review. *Environ Res* 212:113248. <https://doi.org/10.1016/J.ENVRES.2022.113248>
 53. Rajapaksha AU, Chen SS, Tsang DCW et al (2016) Engineered/designer biochar for contaminant removal/immobilization from

- soil and water: potential and implication of biochar modification. *Chemosphere* 148:276–291. <https://doi.org/10.1016/J.CHEMOSPHERE.2016.01.043>
54. Betancur M, Martínez JD, Murillo R (2009) Production of activated carbon by waste tire thermochemical degradation with CO₂. *J Hazard Mater* 168:882–887. <https://doi.org/10.1016/J.JHAZMAT.2009.02.167>
 55. Aworn A, Thiravetyan P, Nakbanpote W (2008) Preparation and characteristics of agricultural waste activated carbon by physical activation having micro- and mesopores. *J Anal Appl Pyrolysis* 82:279–285. <https://doi.org/10.1016/J.JAAP.2008.04.007>
 56. Wu Z, Sun Z, Liu P et al (2020) Competitive adsorption of naphthalene and phenanthrene on walnut shell based activated carbon and the verification: via theoretical calculation. *RSC Adv* 10:10703–10714. <https://doi.org/10.1039/c9ra09447d>
 57. Egbosiuba TC, Abdulkareem AS, Kovo AS, et al (2020) Enhanced adsorption of As(V) and Mn(VII) from industrial wastewater using multi-walled carbon nanotubes and carboxylated multi-walled carbon nanotubes. *Chemosphere* 254. <https://doi.org/10.1016/J.CHEMOSPHERE.2020.126780>
 58. Rashad E, Saleh HN, Eltaweil AS et al (2022) Pinewood sawdust biochar as an effective biosorbent for PAHs removal from wastewater. *Biomass Convers Biorefin*. <https://doi.org/10.1007/s13399-021-02181-7>
 59. Inyang M, Gao B, Zimmerman A et al (2014) Synthesis, characterization, and dye sorption ability of carbon nanotube–biochar nanocomposites. *Chem Eng J* 236:39–46. <https://doi.org/10.1016/J.CEJ.2013.09.074>
 60. Varma AK, Mondal P (2016) Physicochemical characterization and pyrolysis kinetic study of sugarcane bagasse using thermogravimetric analysis. *J Energy Resour Technol, Trans ASME* 138:1–11. <https://doi.org/10.1115/1.4032729>
 61. Sajjadi B, Zubatiuk T, Leszczynska D et al (2019) Chemical activation of biochar for energy and environmental applications: a comprehensive review. *Rev Chem Eng* 35:777–815. <https://doi.org/10.1515/REVCE-2018-0003>
 62. Guo W, Wang S, Wang Y, et al (2018) Sorptive removal of phenanthrene from aqueous solutions using magnetic and non-magnetic rice husk-derived biochars. *R Soc Open Sci* 5. <https://doi.org/10.1098/rsos.172382>
 63. Cardoso NF, Lima EC, Pinto IS et al (2011) Application of cupuassu shell as biosorbent for the removal of textile dyes from aqueous solution. *J Environ Manag* 92:1237–1247. <https://doi.org/10.1016/j.jenvman.2010.12.010>
 64. Haghseresht F, Finnerty JJ, Nouri S, Lu GQ (2002) Adsorption of aromatic compounds onto activated carbons: effects of the orientation of the adsorbates. *Langmuir* 18:6193–6200. <https://doi.org/10.1021/LA025541B>
 65. Yang K, Xing B (2010) Adsorption of organic compounds by carbon nanomaterials in aqueous phase: Polanyi theory and its application. *Chem Rev* 110:5989–6008. https://doi.org/10.1021/CR100059S/ASSET/CR100059S.FP.PNG_V03
 66. Stankovich S, Dikin DA, Piner RD et al (2007) Synthesis of graphene-based nanosheets via chemical reduction of exfoliated graphite oxide. *Carbon N Y* 45:1558–1565. <https://doi.org/10.1016/J.CARBON.2007.02.034>
 67. Chen W, Duan L, Wang L, Zhu D (2008) Adsorption of hydroxyl- and amino-substituted aromatics to carbon nanotubes. *Environ Sci Technol* 42:6862–6868. https://doi.org/10.1021/ES8013612/SUPPL_FILE/ES8013612_SI_001.PDF
 68. Ersan G, Kaya Y, Apul OG, Karanfil T (2015) Adsorption of organic contaminants by graphene nanosheets, carbon nanotubes and granular activated carbons under natural organic matter pre-loading conditions. *Sci Total Environ* 565:811–817. <https://doi.org/10.1016/j.scitotenv.2016.03.224>
 69. Cabal B, Budinova T, Ania CO et al (2009) Adsorption of naphthalene from aqueous solution on activated carbons obtained from bean pods. *J Hazard Mater* 161:1150–1156. <https://doi.org/10.1016/J.JHAZMAT.2008.04.108>
 70. Bergna D, Varila T, Romar H, Lassi U (2018) Comparison of the properties of activated carbons produced in one-stage and two-stage processes. *C (Basel)* 4:41. <https://doi.org/10.3390/c4030041>
 71. Gkika DA, Mitropoulos AC, Kyzas GZ (2022) Why reuse spent adsorbents? The latest challenges and limitations. *Sci Total Environ* 822:153612. <https://doi.org/10.1016/j.scitotenv.2022.153612>
 72. Puzskarewicz A, Kaleta J (2020) The efficiency of the removal of naphthalene from aqueous solutions by different adsorbents. *Int J Environ Res Public Health* 17:1–16. <https://doi.org/10.3390/ijerph17165969>
 73. Chen Z, Chen B, Chiou CT (2012) Fast and slow rates of naphthalene sorption to biochars produced at different temperatures. *Environ Sci Technol* 46:11104–11111. <https://doi.org/10.1021/es302345e>
 74. Owabora CN, Agarry SE, Jato D (2012) Removal of naphthalene from aqueous system using unripe orange peel as adsorbent: effects of operating variables. *Desalination Water Treat* 48:315–319. <https://doi.org/10.1080/19443994.2012.698834>
 75. Yakout SM, Daifullah AAM, El-Reefy SA (2013) Adsorption of naphthalene, phenanthrene and pyrene from aqueous solution using low-cost activated carbon derived from agricultural wastes. *Adsorpt Sci Technol* 31:293–302. <https://doi.org/10.1260/0263-6174.31.4.293>
 76. Kalderis D, Koutoulakis D, Paraskeva P et al (2008) Adsorption of polluting substances on activated carbons prepared from rice husk and sugarcane bagasse. *Chem Eng J* 144:42–50. <https://doi.org/10.1016/j.cej.2008.01.007>
 77. Amin NK (2008) Removal of reactive dye from aqueous solutions by adsorption onto activated carbons prepared from sugarcane bagasse pith. *Desalination* 223:152–161. <https://doi.org/10.1016/j.desal.2007.01.203>
 78. Brandão PC, Souza TC, Ferreira CA et al (2010) Removal of petroleum hydrocarbons from aqueous solution using sugarcane bagasse as adsorbent. *J Hazard Mater* 175:1106–1112. <https://doi.org/10.1016/j.jhazmat.2009.10.060>
 79. Siqueira TCA, da Silva IZ, Rubio AJ, et al (2020) Sugarcane bagasse as an efficient biosorbent for methylene blue removal: kinetics, isotherms and thermodynamics. *Int J Environ Res Public Health* 17. <https://doi.org/10.3390/ijerph17020526>
 80. Mittal A, Mittal J, Malviya A et al (2010) Adsorption of hazardous dye crystal violet from wastewater by waste materials. *J Colloid Interface Sci* 343:463–473. <https://doi.org/10.1016/J.JCIS.2009.11.060>
 81. (17) Preparation and characterization of activated carbon from *Thevetia peruviana* for the removal of dyes from textile waste water | Request PDF. https://www.researchgate.net/publication/267408896_Preparation_and_characterization_of_activated_carbon_from_Thevetia_peruviana_for_the_removal_of_dyes_from_textile_waste_water. Accessed 12 Oct 2022

Publisher's note Springer Nature remains neutral with regard to jurisdictional claims in published maps and institutional affiliations.

Springer Nature or its licensor (e.g. a society or other partner) holds exclusive rights to this article under a publishing agreement with the author(s) or other rightsholder(s); author self-archiving of the accepted manuscript version of this article is solely governed by the terms of such publishing agreement and applicable law.